HEARING THE EDGES: RECOVERING A 3D RECTANGULAR BOX FROM DIRICHLET EIGENVALUES

Eldar Sultanow, Andreas Hatziiliou, and Cornelius May

Abstract. We investigate whether the geometric parameters of a three-dimensional domain can be recovered from the Dirichlet spectrum of the Laplacian. As a controlled benchmark, we consider rectangular boxes, for which the eigenvalues are explicitly known and the Weyl coefficients can be computed in closed form. Exploiting the short-time asymptotics of the heat trace, we extract the leading Weyl coefficients from finite spectral data and show how they encode volume, surface area, and the third spectral Weyl term. These coefficients uniquely determine the side lengths of the box via an explicit cubic reconstruction formula. Numerical experiments based on several thousand eigenvalues demonstrate that the method is stable, accurate, and robust with respect to spectral truncation. The box setting thus provides a stringent validation of the proposed inverse spectral methodology and serves as a foundation for its extension to smooth curved domains, such as triaxial ellipsoids, where explicit spectral formulas are no longer available.

1. The Problem

We consider the Dirichlet spectrum of the Laplacian on a rectangular box

$$\Omega(a,b,c) = \left\{(x,y,z) \in \mathbb{R}^3 : \ 0 < x < a, \ 0 < y < b, \ 0 < z < c\right\} \tag{1}$$

with side lengths $a, b, c > 0$. For the domain $\Omega_{a,b,c} = (0,a) \times (0,b) \times (0,c)$, the Dirichlet eigenvalues separate as in the planar case, see Pinchover and Rubinstein [1, p. 357]:

$$\lambda_{l,n,m} = \left(\frac{l\pi}{a}\right)^2 + \left(\frac{n\pi}{b}\right)^2 + \left(\frac{m\pi}{c}\right)^2, \qquad l,n,m \in \mathbb{N} \tag{2}$$

The corresponding eigenfunctions separate in Cartesian coordinates, and highly accurate spectral data can therefore be generated at negligible computational cost, even for a very large number of eigenvalues. This makes the rectangular box an ideal benchmark geometry for inverse spectral procedures: the geometric invariants which appear in the Weyl and heat-trace asymptotics are known in closed form, while the exact spectrum

2020 *Mathematics Subject Classification.* 35P05, 35P20, 35R30, 35J05, 58J50.

Key words and phrases. Dirichlet spectrum, inverse spectral problem, rectangular box, Weyl asymptotics, heat trace, spectral geometry, geometric reconstruction .

is available without numerical approximation error. However, the domain depends on three independent geometric parameters, rendering it nontrivial from the perspective of the inverse problem.

From this point of view, the task is the following: given a finite subset of the Dirichlet spectrum $\{\lambda_k(\Omega(a,b,c))\}_{k=1}^{N}$, one seeks to recover the side lengths (a,b,c). As in the case of smooth domains, if we are given an ordered list of eigenvalues, the values appearing early on primarily encode coarse geometric information, most notably the volume $V = abc$, while higher spectral modes are required to resolve finer geometric features such as surface area and curvature-related quantities. Although the inverse map from geometry to spectrum is explicitly known in this case, the reconstruction problem still exhibits strong parameter correlations and numerical sensitivity when only *partial* spectral data is available.

2. Methodological steps

The reconstruction procedure consists of three main steps. First, a finite subset of Dirichlet eigenvalues of the Laplacian is generated with high numerical accuracy. Second, the leading Weyl coefficients are extracted from the spectral data by fitting the heat-trace asymptotics in a suitable time window. Finally, the geometric parameters (a,b,c) of the domain are reconstructed from the recovered Weyl coefficients using explicit algebraic relations and a low-dimensional numerical optimization.

2.1. **Generating the eigenvalues.**

For the rectangular box, the Dirichlet eigenvalues of the Laplacian are available in closed form and can therefore be generated with arbitrary accuracy. Exploiting the exact separability of the problem in Cartesian coordinates, the spectrum is obtained by enumerating all admissible integer triples $(l,n,m) \in \mathbb{N}^3$ and evaluating the corresponding eigenvalues as defined by equation (2).

By systematically increasing the truncation bounds for the integer indices, all eigenvalues below a prescribed threshold are captured and subsequently sorted in ascending order. In the numerical experiments reported below, we retain the first few thousand to a few tens of thousands of eigenvalues, which is sufficient to robustly capture the leading terms of the Weyl and heat-trace asymptotics.

2.2. **Extracting the Weyl coefficients.**

The extraction of geometric information from the spectrum is based on the Weyl asymptotics of the counting function $N(\lambda) = \#\{\lambda_k \leq \lambda\}$. For a three-dimensional domain, the leading behavior is governed by the three-term Weyl law for the counting function, see [2, p. 180], [3, p. 37], [4, p. 99]:

$$N(\lambda) = A_0\,\lambda^{3/2} + A_1\,\lambda + A_2\,\lambda^{1/2} + o(\lambda^{1/2}) \tag{3}$$

which defines the Weyl coefficients A_0, A_1, and A_2 used throughout the subsequent reconstruction procedure. While the heat trace of a manifold M is formally defined as the infinite sum $\mathrm{Tr}\big(\mathrm{e}^{t\Delta_M}\big) = \sum_{k=0}^{\infty} \mathrm{e}^{-\lambda_k t}$, see [5, p. 186] and [6, p. 219], its practical numerical evaluation relies on a finite set of N available Dirichlet eigenvalues $\{\lambda_k\}_{k=0}^{N}$. Accordingly, we consider the truncated heat trace

$$Z(t) := \sum_{k=0}^{N} \mathrm{e}^{-\lambda_k t}. \tag{4}$$

In three dimensions, the heat trace admits the well-known short-time asymptotic expansion, obtained by specializing the general heat-trace expansions given in [5, p. 192], [7, p. 272] and [8, p. 53] to dimension $d = 3$:

$$Z(t) \sim \alpha_0\, t^{-3/2} + \alpha_1\, t^{-1} + \alpha_2\, t^{-1/2} + \alpha_3 + \mathcal{O}(t^{1/2}), \tag{5}$$

where the coefficients α_j encode the Weyl data and are directly related to geometric invariants of the domain.

In the numerical setting, the coefficients $\alpha_0, \alpha_1, \alpha_2$, and α_3 are obtained by evaluating the truncated heat trace (4) on a logarithmically spaced short-time grid and fitting it against the basis functions $t^{-3/2}$, t^{-1}, $t^{-1/2}$, and a constant term. The time window is scaled relative to the largest available eigenvalue in order to suppress truncation effects from the finite spectrum.

From the fitted heat coefficients, the Weyl coefficients A_0, A_1, and A_2 are recovered using the global heat-trace asymptotics for $t \to 0^+$, $\sum_{j=0}^{\infty} \mathrm{e}^{-\lambda_j t} = (4\pi t)^{-d/2} \sum_{k\geq 0} a_k\, t^k$, where $d = \dim M$ denotes the spatial dimension; see [5, pp. 189–190]. Since a three-dimensional box (as well as rectangles or disks) is a domain with boundary, in contrast to closed manifolds such as spheres or tori, the heat-trace expansion for manifolds with boundary is required. This heat trace admits an asymptotic expansion with twice as many terms and involves half-integer powers of t, see [5, p. 192]:

$$\sum_{j=1}^{\infty} \mathrm{e}^{-\lambda_j t} \underset{t\to 0^+}{\sim} (4\pi t)^{-\frac{d}{2}} \sum_{k=0}^{\infty} a_{\frac{k}{2}}\, t^{\frac{k}{2}} \tag{6}$$

In our three-dimensional setting, the coefficients appearing in the boundary heat-trace expansion (6) reduce, after specialization to $d = 3$, to the coefficients in (5). These correspond to the appropriately normalized global heat invariants, with $\alpha_0 = (4\pi)^{-3/2} a_0$ and the subsequent coefficients encoding boundary and curvature contributions. These relations follow from the classical correspondence between heat-kernel coefficients and the Weyl expansion of the counting function.

2.3. **Reconstructing the sides.** The coefficients A_0, A_1, A_2 depend on the geometry of the domain and on the imposed boundary conditions. For a rectangular box $\Omega(a,b,c)$ defined by equation (1), the first Weyl coefficient admits the familiar geometric interpretation as the volume of the domain. Indeed, the first Weyl coefficient satisfies $6\pi^2 A_0 = \mathrm{Vol}(\Omega)$, see Safarov and Vassiliev [3, p. xii]. Equivalently, the leading heat invariant satisfies $a_0 = \mathrm{Vol}(\Omega)$, see Levitin et al. [5, p. 190], which in our notation corresponds to $a_0 = \alpha_0(4\pi)^{3/2}$:

$$6\pi^2 A_0 = \alpha_0(4\pi)^{3/2} = \mathrm{Vol}(\Omega) = abc \tag{7}$$

Similarly, the second Weyl coefficient is determined by the surface area of the boundary. For Dirichlet boundary conditions, the corresponding boundary term in the Weyl asymptotic expansion of the counting function is proportional to $\mathrm{Area}(\partial\Omega)$, see [3, p. xii]. Via the classical heat-kernel/Weyl correspondence this yields:

$$-16\pi A_1 = -16\pi\alpha_1 = \mathrm{Area}(\partial\Omega) = 2(ab + ac + bc) \tag{8}$$

The third Weyl coefficient requires special care, since the boundary of a rectangular box is not smooth. As a consequence, the classical interpretation of A_2 in terms of the integrated mean curvature of the boundary does not apply. Instead, the coefficient of the $\lambda^{1/2}$ term is determined spectrally from the exact factorization of the heat trace into one-dimensional Dirichlet heat kernels. This yields an explicit expression for the $t^{-1/2}$ heat coefficient, see Appendix A:

$$\alpha_2^{\mathrm{Weyl}} = \frac{a+b+c}{8\sqrt{\pi}},$$

which represents the genuine third Weyl term for the Dirichlet box. In the normalization adopted in this paper, the corresponding Weyl coefficient A_2 is obtained from α_2^{Weyl} via

$$A_2 = \alpha_2^{\mathrm{Weyl}} \frac{(4\pi)^{3/2}}{4\pi^3} = \frac{a+b+c}{8\sqrt{\pi}} \cdot \frac{(4\pi)^{3/2}}{4\pi^3} = \frac{a+b+c}{4\pi^2} \tag{9}$$

Taken together, the three Weyl coefficients A_0, A_1, A_2 uniquely determine the side lengths (a,b,c) of the rectangular box. By combining the expressions for the Weyl coefficients (7)–(9), we obtain a system of three equations for the three unknown side lengths. Since these expressions correspond to the elementary symmetric polynomials of (a,b,c), Vieta's formulas—see, e.g., Manfrino et al. [9, p. 65] for a pedagogical overview—imply that the side lengths are the three roots of the cubic equation

$$x^3 - (4\pi^2 A_2)\, x^2 + (-8\pi A_1)\, x - (6\pi^2 A_0) = 0. \tag{10}$$

This approach provides a robust method to reconstruct the geometry of the box directly from its heat kernel expansion.

3. Working Example

To illustrate the reconstruction procedure and to provide a fully consistent reference throughout this paper, we consider a fixed rectangular box as a working example. All geometric and spectral quantities used in the following sections are derived from this example. The corresponding side lengths, geometric invariants, and Weyl coefficients are summarized in Table 1.

Table 1. Geometric and spectral features of the example box

Side lengths	$a = 1.0,\ b = 1.5,\ c = 2.3$
Geometric invariants	$\mathrm{Vol} = 3.45,\ \mathrm{Area} = 14.5,\ \int_{\partial\Omega} \bar{H}\,\mathrm{d}S\ =\ 12\pi^2 A_2 = 14.4$
Weyl coefficients	$A_0 = 0.05825968,\ A_1 = -0.28846833,\ A_2 = 0.12158542$

For visual orientation, Figure 1 shows the corresponding box geometry; the corresponding rendering is available on GitHub, see [10]. The illustration highlights the relative proportions of the side lengths and serves as a geometric reference for the numerical reconstruction discussed below.

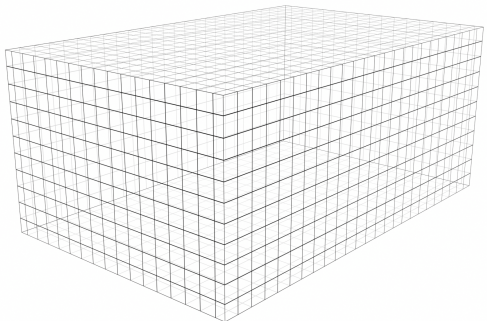

Figure 1. Rectangular box with $a = 1.0$, $b = 1.5$, and $c = 2.3$

3.1. **Generating the eigenvalues.** To generate a sufficiently large and accurate sample of Dirichlet eigenvalues for the rectangular box $\Omega(a, b, c) = (0, a) \times (0, b) \times (0, c)$ with side lengths $a = 1$, $b = 1.5$, and $c = 2.3$, we exploit the exact separability of the Laplacian in Cartesian coordinates. The Dirichlet eigenvalues are given explicitly by equation (2). By enumerating all integer triples (l, n, m) up to a large cutoff and sorting the resulting values in ascending order, we obtain a substantial portion of the low-lying Dirichlet spectrum. In the numerical experiments reported below, we generate 20 000 eigenvalues. The corresponding Mathematica notebook is shown in Listing 1.

LISTING 1. Generation of Dirichlet eigenvalues for the box $\Omega(1, 1.5, 2.3)$.

```
a = 1.0; b = 1.5; c = 2.3; maxIdx = 50;
eigenvalues = Table[Pi^2*((nx/a)^2 + (ny/b)^2 + (nz/c)^2), {nx, 1, maxIdx}, {ny, 1,
    ↪ maxIdx}, {nz, 1, maxIdx}];
lambdaSorted = Sort[Flatten[eigenvalues]][[1 ;; 20000]];
```

The resulting set of eigenvalues is exported to a text file for subsequent processing. The notebook used to generate the spectrum is available on GitHub, see [11]. For reference, the first 15 and the last 5 eigenvalues of the 20 000 generated values are

16.121804,	21.718934,	29.281277,	31.047482,	34.878406,
44.107450,	44.206955,	45.730618,	51.213731,	51.327747,
56.810860,	57.266923,	58.890090,	60.656295,	60.898838,
		...		
5142.949068,	5143.034062,	5143.471467,	5143.471467,	5143.929602

3.2. **Extracting the Weyl coefficients.** Starting from the numerically generated Dirichlet spectrum $\{\lambda_k\}_{k=1}^{20000}$, the Weyl coefficients are extracted via the short-time asymptotics of the heat trace given by the sum (4). Rather than fitting the counting function $N(\lambda)$ directly, the heat-trace approach provides improved numerical stability and allows for a clean separation of the different asymptotic contributions.

3.2.1. *Choice of the time window.* Since only a finite portion of the spectrum is available, the time interval $[t_{\min}, t_{\max}]$ must be chosen carefully. To suppress contributions from the truncated spectral tail, the window is scaled relative to the largest eigenvalue λ_N according to

$$t_{\min} = \frac{f_{\min}}{\lambda_N}, \qquad t_{\max} = \frac{f_{\max}}{\lambda_N},$$

with fixed dimensionless factors $f_{\min}$ and $f_{\max}$. For the present example with $N = 20\,000$ eigenvalues, we use $f_{\min} = 35$ and $f_{\max} = 350$, ensuring that $\mathrm{e}^{-\lambda_N t}$ is negligible throughout the fitting range. The heat trace is evaluated on a logarithmically spaced grid of 251 points within this interval.

3.2.2. *Heat-trace fit.* As introduced in equations (4) and (5), the Weyl coefficients are recovered from the fitted heat-trace coefficients α_j. Numerically, the coefficients $\alpha_0, \alpha_1, \alpha_2, \alpha_3$ are obtained by a linear least-squares fit of the computed heat trace against the basis functions $t^{-3/2}$, t^{-1}, $t^{-1/2}$, and a constant term. This results in a small overdetermined linear system, which is solved using the pseudoinverse, as implemented in Listing 2.

LISTING 2. Heat-trace evaluation and linear fit.

```
λN = Last[eigs];
fMin = 35;
fMax = 350;
fGrid = 250;
tMin = fMin/λN;
tMax = fMax/λN;
tGrid = Exp@Subdivide[Log[tMin], Log[tMax], fGrid];
Z = Total[Exp[-Outer[Times, eigs, tGrid]], {1}];
X = Table[t^{-3/2, -1, -1/2, 0}, {t, tGrid}];
{α0, α1, α2, α3} = PseudoInverse[X].Z;
```

3.2.3. *Conversion to Weyl coefficients.* The coefficients obtained from the heat-trace fit are related to the Weyl coefficients through the standard correspondence between heat-kernel asymptotics and the spectral counting function. In the normalization adopted throughout this paper, the leading coefficient α_0 determines the volume term via equation (7), while the coefficient α_1 yields the surface-area contribution according to equation (8). The numerical extraction of the heat coefficients α_j is performed by a linear least-squares fit of the truncated heat trace, as described above and implemented in Listing 2; their conversion into Weyl coefficients is carried out in Listing 3.

The third Weyl coefficient requires special care for the rectangular box, since the boundary is not smooth and the classical geometric interpretation in terms of integrated mean curvature does not apply. Instead, the coefficient of the $t^{-1/2}$ term is determined spectrally from the exact factorization of the Dirichlet heat trace. This yields the genuine Weyl coefficient α_2^{Weyl}, from which A_2 follows via equation (9). The numerical extraction and conversion of this term are handled analogously and are included in Listings 2 and 3.

LISTING 3. Conversion from heat coefficients to Weyl coefficients.

```
A0hat = (α0*(4 Pi)^(3/2))/(6 Pi^2);
A1hat = α1;
A2hat = (α2*(4 Pi)^(3/2))/(4 Pi^3);
```

3.2.4. *Validation against exact values.* For the rectangular box, all Weyl coefficients are known in closed form. This allows for a direct and unambiguous validation of the spectral extraction procedure. In particular, the first and second coefficients correspond to the volume and surface area of the domain, while the third coefficient incorporates the non-smooth edge contribution characteristic of polyhedral boundaries.

Table 2 compares the Weyl coefficients and the associated geometric invariants obtained from the heat-trace fit against their exact theoretical values. For all quantities

considered, the relative deviation remains below 10^{-3}, demonstrating excellent agreement. This confirms that the proposed heat-based extraction method recovers not only the leading volume and surface terms, but also the subtle third Weyl coefficient associated with edge effects, with high numerical accuracy.

TABLE 2. Validation of spectrally extracted Weyl coefficients against exact values for the rectangular box.

Geometric quantity	Extracted ($N = 20\,000$)	Exact	Relative error (%)
Volume V	3.45	3.45	-0.0000128368
Surface area S	14.5	14.5	-0.0000875185
Edge curvature integral $12\pi^2 A_2$	14.3999	14.4	-0.000606245
A_0 (spectral)	0.0582597	0.0582597	-0.0000128368
A_1 (spectral)	-0.288468	-0.288468	-0.0000875185
A_2 (spectral)	0.121585	0.121585	-0.000606245

3.3. **Reconstructing the sides.** Once the Weyl coefficients A_0, A_1, and A_2 have been extracted from the spectrum, the reconstruction of the side lengths a, b, c reduces to solving a single cubic equation. As shown in Section 2.3, the side lengths are given by the three positive real roots of the polynomial (10).

In practice, the roots of this equation are computed numerically. Since the rectangular box yields three strictly positive real solutions, the reconstructed side lengths are obtained by taking the real parts of the roots and sorting them in ascending order. The corresponding implementation in MATHEMATICA is shown in Listing 4.

LISTING 4. Reconstruction procedure based on the Weyl coefficients.

```
e1 = 4 Pi^2*A2hat;
e2 = -8 Pi*A1hat;
e3 = 6 Pi^2*A0hat;

poly = x^3 - e1*x^2 + e2*x - e3;
rootsComplex = x /. NSolve[poly == 0, x];
sideLengthsRec = Sort[Re[rootsComplex]];
```

Table 3 summarizes the reconstructed side lengths obtained from the spectrally extracted Weyl coefficients and compares them to the exact geometric values. All three side lengths are recovered with relative errors below 10^{-4}, confirming the accuracy and numerical stability of the reconstruction procedure.

TABLE 3. Side lengths reconstructed via Listing 4.

Side length	Reconstructed	Exact	Deviation
a	0.999964	1.0	−0.0000356821
b	1.50014	1.5	0.000141013
c	2.29987	2.3	−0.00013443

4. CAN FEWER EIGENVALUES SUFFICE?

A natural practical question is how many Dirichlet eigenvalues are required in order to reliably extract the Weyl coefficients, in particular the third coefficient A_2, which is known to be the most sensitive to truncation effects and numerical noise.

To address this question, we repeat the heat-trace based extraction procedure for progressively smaller subsets of the spectrum. Starting from the full set of 20 000 eigenvalues, we truncate the spectrum to $N = 10\,000$, $5\,000$, and $2\,000$ eigenvalues, and study the relative error in the reconstructed coefficient A_2 as a function of the lower bound $t_{\min}$ of the heat-trace fitting window. In all cases, the upper bound is chosen sufficiently large to suppress higher-order terms of the heat expansion. For each truncation level N, the relative error in A_2 exhibits a pronounced stability minimum as $t_{\min}$ is varied.

A robust empirical scaling is that the optimal lower bound scales with the inverse of the largest available eigenvalue,

$$t_{\min}^{*} \approx \frac{c(N)}{\lambda_N} \tag{11}$$

where the dimensionless constant $c(N) = t_{\min}^{*}\lambda_N$ depends on the truncation level and, as we show later, on the box aspect ratios. For the reduced spectrum with $N = 2000$ eigenvalues in our working example, we observe $c(2000) \approx 69$. This scaling law is clearly visible in Figure 2, which shows the relative error of A_2 as a function of the dimensionless parameter $f = t_{\min}\lambda_N$ for different truncation levels. In particular, we find that already $N \approx 2\,000$ eigenvalues are sufficient to recover A_2 with relative errors below one percent, provided the fitting window is chosen according to equation (11). This demonstrates that the proposed procedure does not require extremely large spectral data sets, and that the third Weyl coefficient can be extracted robustly even from moderately sized spectra, as long as the time window is selected in a controlled manner.

As shown in Figure 2, all curves exhibit a pronounced stability minimum, reflecting the balance between truncation errors at very small times and the influence of subleading heat terms at larger times. However, the location of the minimum is *not* universal

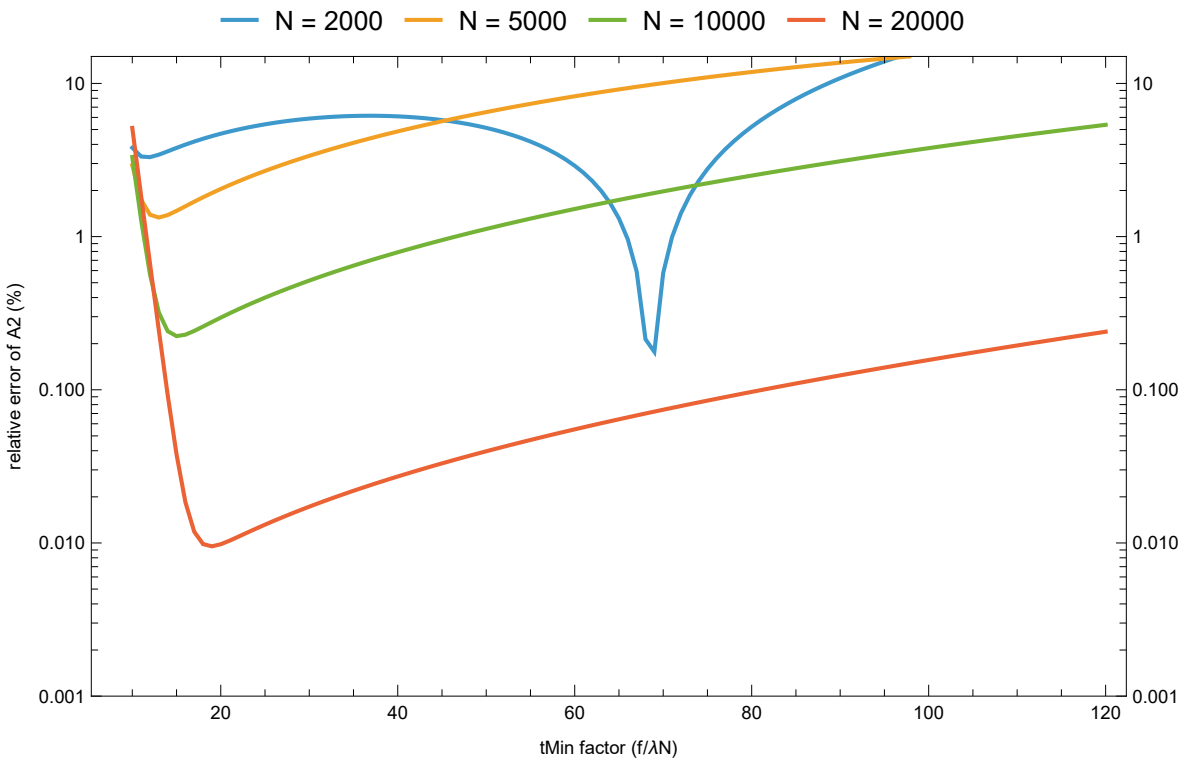

FIGURE 2. Relative error of the reconstructed Weyl coefficient A_2 as a function of the dimensionless parameter $f = t_{\min}\lambda_N$ for different truncation levels N.

across truncation levels: the optimal dimensionless cutoff $f^*(N) = t^*_{\min}\lambda_N$ depends noticeably on N for the present data set. In particular, in Figure 2 the minimizer shifts to smaller values of f as more eigenvalues are included, while for the most strongly truncated spectrum ($N = 2000$) the minimum occurs near $f^* \approx 69$.

Guided by Figure 2, we choose $f_{\min} = 69$ for the reduced experiment with $N = 2000$ eigenvalues, since this value is near the observed stability minimum in that truncation regime. We keep $f_{\max} = 500$ and use a logarithmic grid with 251 sampling points. We then repeat the full extraction and reconstruction procedure using only the first $N = 2\,000$ Dirichlet eigenvalues.

Despite the substantial reduction of spectral input data, the reconstructed Weyl coefficients remain in very good agreement with their exact values. In particular, the third Weyl coefficient A_2, which is most sensitive to truncation effects, is recovered with

a relative error well below one percent. The resulting geometric quantities derived from the Weyl coefficients show comparable accuracy; see Table 4.

These results demonstrate that the proposed heat-trace based extraction of Weyl coefficients remains robust even when only a few thousand eigenvalues are available. In particular, once the stability minimum of the heat-time window is respected, no fine tuning of parameters is required. This makes the method well suited for applications in which the numerical computation of very high eigenvalues is prohibitively expensive, such as curved or non-separable geometries.

TABLE 4. Reconstruction of Weyl coefficients and derived geometric quantities for the rectangular box using a reduced spectral input ($N = 2\,000$ eigenvalues).

Geometric quantity	Reconstructed ($N = 2000$)	Exact	Relative error (%)
Volume V	3.47998	3.45	0.86
Surface area S	14.6822	14.5	1.25
Edge curvature integral $12\pi^2 A_2$	14.4255	14.4	0.17
A_0 (spectral)	0.0587659	0.0582597	0.86
A_1 (spectral)	−0.292094	−0.288468	1.25
A_2 (spectral)	0.121801	0.121585	0.17

4.1. **A stability landscape across box aspect ratios.** So far an empirical scaling rule $t^*_{\min}\lambda_N \approx 69$ has been established for the working example $\Omega(1, 1.5, 2.3)$. We now probe how universal this constant is by repeating the stability-minimum search across a wide family of rectangular boxes.

The Dirichlet spectrum of a box is invariant under uniform scaling in the sense that $\lambda_k(\Omega(\alpha a, \alpha b, \alpha c)) = \alpha^{-2}\lambda_k(\Omega(a, b, c))$. Hence, it suffices to fix $a = 1$ and to parameterize shapes by the aspect ratios

$$x = \frac{b}{a}, \qquad y = \frac{c}{a}.$$

We sample (x, y) on a 200×200 logarithmic grid in the range $x, y \in [0.3, 3.0]$. For each shape $\Omega(1, x, y)$, we generate the first $N = 2000$ exact eigenvalues from (2).

Let us approach a definition of the stability minimum f^*. For a fixed spectrum truncation N, we evaluate the truncated heat trace $Z(t) = \sum_{k=1}^{N} e^{-\lambda_k t}$ on a logarithmic time grid over $t \in [t_{\min}, t_{\max}]$ with

$$t_{\min} = \frac{f}{\lambda_N}, \qquad t_{\max} = \frac{500}{\lambda_N},$$

and we perform a four-term heat-trace fit $\alpha_0 t^{-3/2} + \alpha_1 t^{-1} + \alpha_2 t^{-1/2} + \alpha_3$ by linear least squares. From the fitted coefficient α_2 we obtain the spectral estimate

$$\widehat{A}_2(f) = \frac{\alpha_2 (4\pi)^{3/2}}{4\pi^3}$$

which can then be compared to the exact expression (9). For the Dirichlet box, the third Weyl coefficient is known as $A_2 = \frac{a+b+c}{4\pi^2} = \frac{1+x+y}{4\pi^2}$; see equation (9). We therefore scan $f \in \{1, 2, \ldots, 200\}$ and define the stability minimum as

$$f^*(x,y) = \arg\min_f \left| \frac{\widehat{A}_2(f)}{A_2} - 1 \right|$$

From a numerical perspective, the heat-trace fit underlying the definition of f^* can be viewed as a linear regression problem. For each choice of $t_{\min}$, the sampled heat trace values $Z(t_j)$ are assembled into a data vector, while the corresponding design (feature) matrix is given by

$$X = \begin{pmatrix} t_1^{-3/2} & t_1^{-1} & t_1^{-1/2} & 1 \\ t_2^{-3/2} & t_2^{-1} & t_2^{-1/2} & 1 \\ \vdots & \vdots & \vdots & \vdots \\ t_M^{-3/2} & t_M^{-1} & t_M^{-1/2} & 1 \end{pmatrix},$$

where $\{t_j\}_{j=1}^M$ denotes the logarithmically spaced time grid. The heat coefficients $(\alpha_0, \alpha_1, \alpha_2, \alpha_3)$ are then obtained by solving the overdetermined linear system $X\,\alpha \approx Z$ in the least-squares sense. The stability minimum f^* thus identifies the regime in which this regression problem is optimally conditioned with respect to the extraction of the coefficient α_2, and hence of the Weyl coefficient A_2.

Figure 3 visualizes the map $(x, y) \mapsto f^*(x, y)$ as a 3D surface, generated with the notebook [12]. Rather than a single universal constant, f^* depends strongly on the aspect ratios. Moderately anisotropic boxes cluster around $f^* \approx 60$ to 80, including the working example $\Omega(1, 1.5, 2.3)$ with $f^* \approx 69$. Near the isotropic cube regime $x \approx y \approx 1$, forming a shallow basin in the stability landscape, the optimum drops markedly to $f^* \approx 14$. For highly anisotropic boxes (one side much smaller than the other), f^* decreases again and can reach values close to the lower end of our scan. By symmetry, the landscape is invariant under swapping x and y and overall exhibits a pronounced ridge-and-crater structure reminiscent of a "volcano".

Here, $f^* = t_{\min}\lambda_N$ denotes the dimensionless heat-time cutoff that minimizes the relative error of the reconstructed third Weyl coefficient A_2 in a four-term heat-trace fit based on $N = 2000$ eigenvalues.

The stability-minimum search remains robust and inexpensive (it requires only a one-dimensional scan in f once the spectrum is available), and it provides an automatic geometry-adaptive choice of $t_{\min}$ for truncated spectral data.

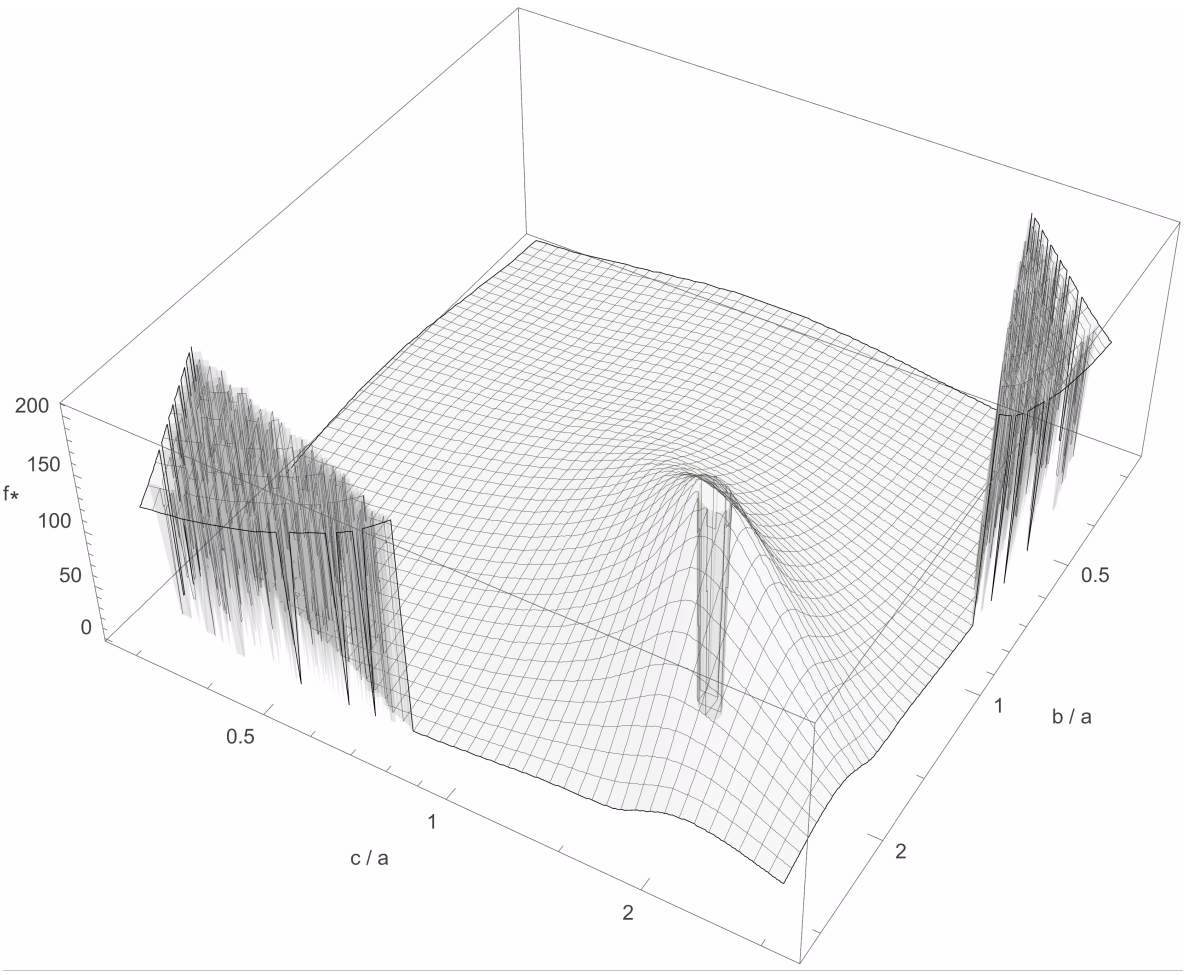

FIGURE 3. Stability landscape $f^*(x, y)$ for the Dirichlet box with $a = 1$

4.2. **Stability Minimum from Optimal Truncation in Laplace-Type Asymptotics.** We observed the robust empirical scaling law (11), namely $t^*_{\min} \approx c(N)/\lambda_N$, i.e. the optimal lower cutoff scales inversely with the largest available eigenvalue. Hence the stability minimum is governed by the dimensionless combination $f^* = t^*_{\min}\lambda_N \approx c(N)$. For $N = 2000$ eigenvalues we obtain numerically $f^* \approx 69$. We now provide a heuristic explanation of this dimensionless constant in terms of optimal truncation in Laplace-type asymptotics.

Bender and Orszag analyze integrals of the form $I(x) = \int f(t)e^{x\phi(t)}\,dt$ as $x \to \infty$, see [13, p. 261]. On p. 267 they derive the leading asymptotic contribution in the case when ϕ has a non-degenerate interior maximum at $c \in (a, b)$, so that $\phi'(c) = 0$ and $\phi''(c) < 0$. For $x \to +\infty$ this yields

$$I(x) \sim \frac{\sqrt{2\pi}\, f(c)\, e^{x\phi(c)}}{\sqrt{-x\,\phi''(c)}} = \left(\sqrt{2\pi}\, f(c)\, \frac{1}{\sqrt{-\phi''(c)}}\right) e^{x\phi(c)} x^{-1/2} = K e^{x\phi(c)} x^{-1/2} \tag{12}$$

Defining the x-independent prefactor K, we obtain the structural form $I(x) \sim K e^{x\phi(c)}\, x^{-1/2}$, that is, an exponential factor multiplied by the algebraic prefactor $x^{-1/2}$ with an x-independent constant K. In our cutoff problem the relevant contribution is exponentially *suppressed*. We therefore rewrite the exponent in (12) in decay form by setting $\phi(c) = -\psi$ with $\psi > 0$, so that $e^{x\phi(c)} = e^{-x\psi}$. This yields $I(x) \sim K\, e^{-x\psi}\, x^{-1/2}$.

For the balance argument only the exponential–algebraic structure matters; the x-independent constant K and the precise value of ψ are not essential. We therefore reduce the expression to the structural template $I(x) \sim e^{-x\psi}\, x^{\alpha}$ as $x \to \infty$, with an algebraic exponent α determined by the specific setting (for Laplace's method in the non-degenerate case, $\alpha = -1/2$). Note that although the heat trace itself is analyzed in the short-time regime $t \to 0^+$, the relevant asymptotic parameter in the truncated tail is the dimensionless quantity $f = t\lambda_N$. In the stability-minimum regime one has $f \to \infty$, so f plays precisely the role of the large parameter x in Laplace's method.

Using Weyl's law in three dimensions (Appendix C), the truncated spectral tail admits the representation $R_{\text{trunc}}(t) \sim t^{-3/2}\Gamma\big(\frac{3}{2}, f\big)$. Hence the tail inherits the same "exponential times power" structure. In particular, for large f, $\Gamma\big(\frac{3}{2}, f\big) \sim f^{1/2}e^{-f}$, which is precisely of the form $e^{-x\psi}x^{\alpha}$ (with $x \leftrightarrow f$ and $\alpha = 1/2$).

A central message here is the principle of *optimal truncation*: asymptotic approximations are most accurate when truncated near the point where the exponentially small remainder becomes comparable (in its effect) to algebraic contributions; beyond that point the remainder grows again. In our problem, the finite-eigenvalue approximation introduces a truncated spectral tail whose asymptotic behaviour was derived above. For large f, the dominant contribution is of the form $f^{1/2}e^{-f}$, i.e. it has the Laplace-type

"exponential times power" structure. Since our regression model uses only finitely many heat terms, the first neglected contribution scales algebraically like $t^{1/2} = (f/\lambda_N)^{1/2}$.

According to the optimal truncation principle, the stability minimum occurs when the exponentially suppressed tail contribution and the algebraic model contribution have comparable influence on the regression. Balancing the dominant factors gives $f^{1/2}e^{-f} \sim \lambda_N^{-1/2} f^{-1/2}$, and hence the structural balance equation $fe^{-f} \sim \lambda_N^{-1/2}$. Taking natural logarithms yields $-f + \log f = -\frac{1}{2}\log\lambda_N + \text{const}$, or equivalently the implicit form

$$f = \tfrac{1}{2}\log\lambda_N + \log f + \text{const}. \tag{13}$$

This has the characteristic signature of exponential–algebraic competition: the exponential term produces a linear dependence on f after taking logs, while algebraic contributions enter only through logarithmic corrections. In our experiment, $\lambda_N \approx 5143$ and $\frac{1}{2}\log\lambda_N \approx 4.27$. For $f \approx 70$ one has $\log f \approx 4.25$, so the logarithmic contributions in (13) account for roughly 8.5.

The constant in (13) is not a small correction but represents the logarithm of an effective prefactor in the balance equation. More precisely, the structural relation $fe^{-f} \sim C_{\text{eff}}\,\lambda_N^{-1/2}$ leads after taking natural logarithms to $f = \frac{1}{2}\log\lambda_N + \log f - \log C_{\text{eff}}$. Hence the constant term equals $-\log C_{\text{eff}}$. For our numerical values ($f^* \approx 69$, $\lambda_N \approx 5143$) one obtains $C_{\text{eff}} \approx fe^{-f}\sqrt{\lambda_N} \approx 5 \times 10^{-27}$, so that $-\log C_{\text{eff}} \approx 60.5$. This effective prefactor collects geometric constants (from Weyl asymptotics and the Γ-expansion) as well as the sensitivity of the least-squares regression.

In summary, the stability minimum is naturally interpreted as an instance of optimal truncation in Laplace-type asymptotics: the reconstruction error is minimized at the point where exponentially suppressed spectral-tail effects balance algebraically growing model errors, consistent with the general principles described in [13].

4.3. **Analytic structure of the baseline contour $f^* = 69$.** To better understand when the one-parameter rule of thumb $f = 69$ is reliable, we consider the iso-contour

$$\Gamma_{69} = \{(x, y) \in [0.3, 3]^2 : \ f^*(x, y) = 69\}$$

in the stability landscape shown in Figure 3. Here $x = b/a$ and $y = c/a$ denote the aspect ratios of the box $\Omega(a, b, c)$ with $a = 1$. Empirically, Γ_{69} forms a closed curve surrounding the near-cube regime. It separates geometries for which the constant baseline $f = 69$ performs well from regimes in which a geometry-adaptive choice of $f^*(x, y)$ becomes preferable. In logarithmic aspect-ratio coordinates

$$u = \frac{\log x + \log y}{\sqrt{2}}, \qquad v = \frac{\log x - \log y}{\sqrt{2}},$$

the contour exhibits a structured but slightly asymmetric shape. While a simple ellipse gives a rough approximation, the stability contour is more accurately captured by the implicit relation (14), defining the region where the constant cutoff $f = 69$ is near-optimal for recovering A_2. As shown in Appendix B, this contour defines a rational algebraic plane curve of degree four that is birationally equivalent to a conic:

$$\frac{(u - u_0)^2}{\big(a_0(1 + \kappa(u - u_0))\big)^2} + \frac{v^2}{b_0^2} = 1, \tag{14}$$

where the fitted parameters are $u_0 = 0.239$, $a_0 = 0.927$, $b_0 = 0.601$ and $\kappa = -0.339$. In the limit $\kappa = 0$, equation (14) reduces to an ordinary ellipse. The additional factor in the denominator introduces a controlled deformation along the diagonal direction u, producing the empirically observed slightly egg-shaped contour. The model respects the symmetry under exchange $x \leftrightarrow y$, corresponding to $v \mapsto -v$, while allowing for anisotropic skewness along the u-direction. Numerically, the approximation achieves a root-mean-square deviation of approximately RMSE ≈ 0.013 with respect to the extracted $z \approx 69$ plateau, indicating that the contour is not merely elliptic but exhibits a reproducible and structured deformation.

Figure 4 shows the extracted $f^* = 69$ plateau in (u, v)-coordinates together with the fitted egg-shaped contour (14) as computed by the notebook [14].

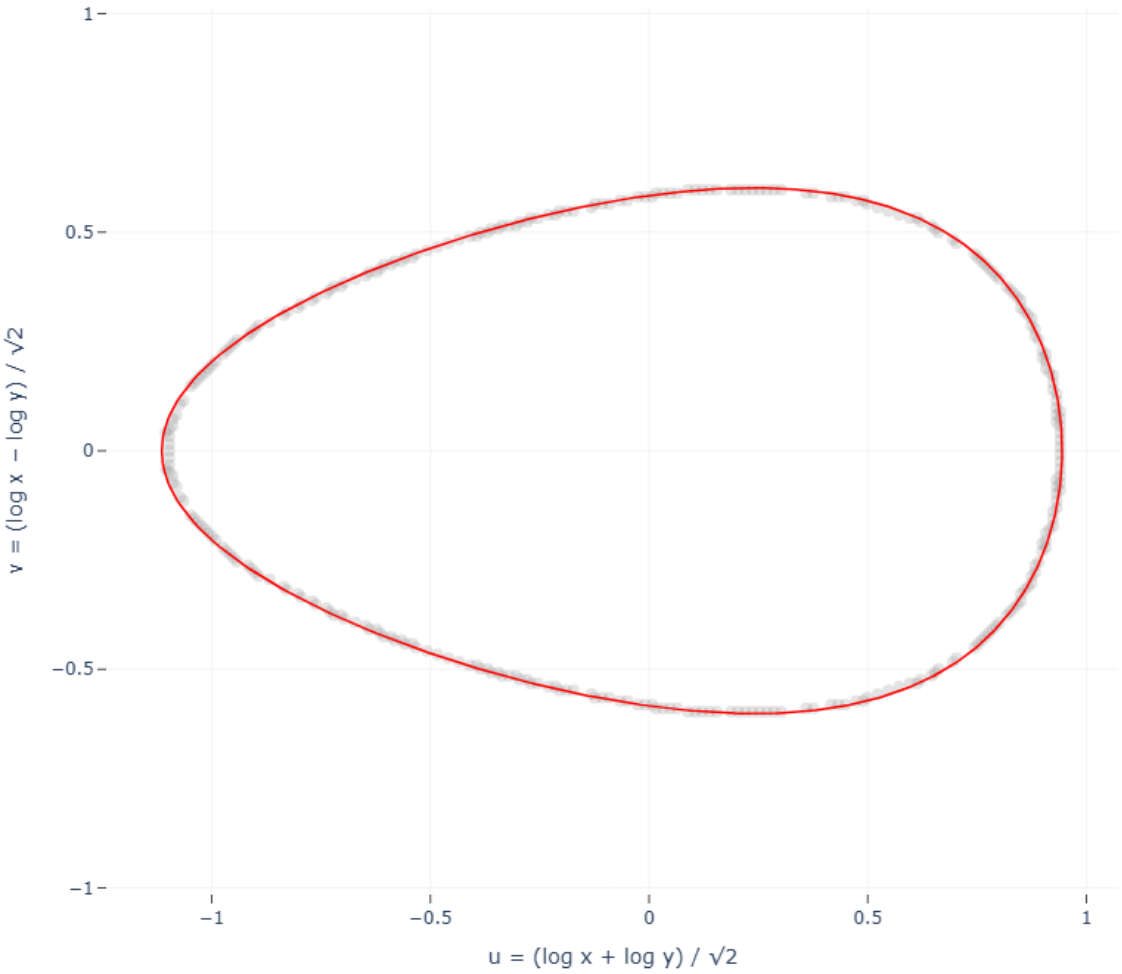

FIGURE 4. Stability plateau $f^* = 69$ in (u, v)-coordinates together with the fitted implicit contour (14).

5. Outlook and Further Research

The reconstruction methodology presented in this work is deliberately validated on rectangular boxes, where exact spectral data and explicit Weyl coefficients are available. Having established the accuracy and stability of the approach in this controlled setting, a natural next step is its application to smooth curved domains, such as ellipsoids or more general convex bodies, for which no closed-form eigenvalue expressions

exist. In such cases, the third Weyl coefficient regains its classical geometric interpretation in terms of the integrated mean curvature of the boundary, providing direct access to curvature-related shape information. Extending the present framework to these geometries requires high-accuracy numerical eigenvalue computations on curved domains.

Another natural direction for further research concerns the *a-priori* determination of the optimal fitting window for truncated heat trace data. In the present work, the lower bound $t_{\min}$ is chosen empirically by identifying a stability minimum in the reconstructed coefficient A_2, which consistently occurs at the dimensionless value $t_{\min}\lambda_N \approx 69$ for the rectangular box. This behavior suggests that the optimal choice of $t_{\min}$ is governed by a dimensionless balance between truncation effects due to the finite number of eigenvalues and deviations from the short-time heat trace asymptotics at larger times. A systematic modeling of this trade-off may lead to a predictive and fully automatic criterion for selecting the fitting interval, avoiding visual inspection or prior calibration. Such an approach promises improved robustness and may generalize naturally to other geometries, higher dimensions, and different spectral truncation regimes.

Acknowledgements

I am grateful to Prof. Elmar Schrohe for suggesting the study of inverse spectral questions, for inspiring the investigation of how geometric information can be recovered from eigenvalue data, and for his valuable support.

Appendix A. Derivation of the third Weyl coefficient for the Dirichlet box

We derive the explicit expression for the third Weyl coefficient of a rectangular box $\Omega(a,b,c)$ with Dirichlet boundary conditions. The derivation relies on the exact factorization of the heat trace into one-dimensional contributions and makes explicit the origin of the additional term arising from the non-smooth boundary of the box. We follow the general definition of the heat trace introduced in Section 2.2. For the Dirichlet Laplacian on an interval $(0,a)$, we denote the associated heat trace by $Z_a(t) = \mathrm{Tr}\big(\mathrm{e}^{t\Delta_{(0,a)}}\big)$.

Since the spectrum of the one-dimensional Dirichlet Laplacian on an interval of length a is explicitly given by $\lambda_n = \pi^2 n^2/a^2$, $n \geq 1$, see [15, p. 322] and [16, p. 283], the heat trace can be written as

$$Z_a(t) = \sum_{n=1}^{\infty} \exp\left(-\frac{\pi^2 n^2}{a^2} t\right) \tag{15}$$

In the presence of a boundary, we need to use the asymptotic expansion (6). Restricting the inner sum to its first two algebraic terms, corresponding to $k=0$ and $k=1$, yields the one-dimensional Dirichlet contribution $(4\pi t)^{-1/2}\big(a_0 + a_{1/2}\, t^{1/2}\big)$ and hence $\frac{a}{\sqrt{4\pi t}} - \frac{1}{2}$ after inserting $a_0 = \mathrm{Vol}(M) = a$ and $a_{1/2} = -\sqrt{\pi}$. Here the limit $t \to 0^+$ is understood, while the remaining contributions are exponentially suppressed. The leading coefficient equals the volume of M, whereas the terms with half-integer powers arise from boundary contributions. As shown in [5, p. 192], for Dirichlet boundary conditions one has

$$a_{\frac{1}{2}} = -\frac{\sqrt{\pi}}{2}\,\mathrm{Vol}_{d-1}(\partial M). \tag{16}$$

In our one-dimensional setting[1] $M = (0,a)$, we have $d=1$, $\mathrm{Vol}(M) = a$, and $\mathrm{Vol}_{d-1}(\partial M) = \mathrm{Vol}_0(\partial M) = 2$. Inserting these values into (16) yields $a_{1/2} = -\sqrt{\pi}$. Substituting this coefficient into the prefactor $(4\pi t)^{-1/2}$ of equation (6) then gives

$$Z_a(t) \underset{t\to 0^+}{\sim} \frac{1}{\sqrt{4\pi t}}\big(a_0 + a_{\frac{1}{2}} t^{\frac{1}{2}}\big) = \frac{1}{\sqrt{4\pi t}}\big(a - \sqrt{\pi}\, t^{\frac{1}{2}}\big) = \frac{a}{\sqrt{4\pi t}} - \frac{1}{2} + \mathcal{O}\Big(\mathrm{e}^{-\frac{a^2}{4t}}\Big) \tag{17}$$

which is precisely the short-time asymptotic expansion used in the subsequent factorization argument. The constant term $-1/2$ reflects the presence of the Dirichlet boundary. For the rectangular box $\Omega(a,b,c) = (0,a)\times(0,b)\times(0,c)$, separation of

[1] In this context Vol_0 denotes the 0-dimensional Hausdorff measure. For $M = (0,a) \subset \mathbb{R}$ the boundary consists of two points, $\partial M = \{0,a\}$, and thus $\mathrm{Vol}_0(\partial M) = 2$.

variables and the explicit one-dimensional heat trace (15), which legitimizes the product structure, imply an exact factorization of the heat trace, $Z_\Omega(t) = Z_a(t)\, Z_b(t)\, Z_c(t)$, where $Z_b(t)$ and $Z_c(t)$ are defined analogously. Writing $Z_a(t) = A\, t^{-1/2} - \frac{1}{2} + \cdots$ with $A = a/\sqrt{4\pi}$ (and similarly $B = b/\sqrt{4\pi}$, $C = c/\sqrt{4\pi}$), we obtain

$$Z_\Omega(t) = (At^{-1/2} - \tfrac{1}{2})(Bt^{-1/2} - \tfrac{1}{2})(Ct^{-1/2} - \tfrac{1}{2}) + \cdots .$$

Expanding this product yields

$$Z_\Omega(t) \sim ABC\, t^{-3/2} - \frac{1}{2}(AB + AC + BC)\, t^{-1} + \frac{1}{4}(A + B + C)\, t^{-1/2} - \frac{1}{8} + \cdots .$$

Consequently, the coefficient of the $t^{-1/2}$ term is given by

$$\alpha_2^{\mathrm{Weyl}} = \frac{1}{4}(A + B + C) = \frac{1}{4}\left(\frac{a+b+c}{\sqrt{4\pi}}\right) = \frac{a+b+c}{8\sqrt{\pi}}.$$

Appendix B. Conic Reduction of Stability Boundaries

We start from the implicit stability relation (14). For notational simplicity, we introduce the shifted coordinate $x := u - u_0$ and set $y := v$. Equation (14) then takes the form

$$\frac{x^2}{a_0^2(1+\kappa x)^2} + \frac{y^2}{b_0^2} = 1. \tag{18}$$

Rational plane curves admit representations of the form (19), where $X(u)$, $Y(u)$ and $W(u)$ are polynomials sharing a common denominator (cf. Piegl & Tiller [17, p. 26]).

$$x(u) = \frac{X(u)}{W(u)}, \qquad y(u) = \frac{Y(u)}{W(u)}. \tag{19}$$

In the present case, the nonlinear deformation of the ellipse is entirely induced by the rational factor $(1+\kappa x)^{-1}$ in the x-coordinate. This suggests introducing the rational change of variable

$$\xi = \frac{x}{1+\kappa x}, \qquad x = \frac{\xi}{1-\kappa\xi} \tag{20}$$

Substituting $x = \xi/(1-\kappa\xi)$ into (18) eliminates the rational deformation and yields $\xi^2/a_0^2 + y^2/b_0^2 = 1$, an ellipse.

Since both maps are rational inverses of each other, the two curves are birationally equivalent. There is only one conic in a projective plane, i.e., all nondegenerate (smooth) projective conics are projectively equivalent [18, p. 252]. Such a conic is rational and birational to the projective line $\mathbb{P}^1$ [19, p. 73]. Since $\mathbb{P}^1$ has genus 0 [20, p. 548] and birational transformation conserves the genus [21, p. 544], [22, p. 179], any smooth conic and thus the stability boundary is likewise a genus-zero curve. Clearing denominators in the equation (18) yields a quartic, that is a polynomial equation in (x, y) of total degree four. As the coordinate change (20) is a birational self-map of the projective plane, it lies in the Cremona group (cf. [23, p. 29]), so the quartic stability boundary arises from a conic via a Cremona transformation.

Appendix C. Derivation of the $\Gamma(\frac{3}{2}, f)$-Structure from Weyl's Law

We briefly justify the appearance of the exponent $3/2$ in the incomplete Gamma function governing the truncated spectral tail. In dimension $d = 3$, Weyl's law implies that the spectral density satisfies $\rho(\lambda) \sim C\,\lambda^{1/2}$ as $\lambda \to \infty$ for some geometry-dependent constant C. Replacing the discrete spectral tail by its integral approximation, we obtain

$$\sum_{\lambda_k > \lambda_N} e^{-t\lambda_k} \;\approx\; \int_{\lambda_N}^{\infty} \rho(\lambda) e^{-t\lambda}\, d\lambda \sim C \int_{\lambda_N}^{\infty} \lambda^{1/2} e^{-t\lambda}\, d\lambda.$$

With the change of variables $u = t\lambda$, $d\lambda = \frac{du}{t}$ and $\lambda = \frac{u}{t}$, the integral becomes

$$C \int_f^{\infty} \left(\frac{u}{t}\right)^{1/2} e^{-u} \frac{du}{t} = C\, t^{-3/2} \int_f^{\infty} u^{1/2} e^{-u}\, du, \qquad f = t\lambda_N.$$

The remaining integral is precisely the upper incomplete Gamma function, $\Gamma\left(\frac{3}{2}, f\right) = \int_f^{\infty} u^{1/2} e^{-u}\, du$. Hence $R_{\text{trunc}}(t) \sim C\, t^{-3/2} \Gamma\left(\frac{3}{2}, f\right)$. In general dimension d, Weyl's law gives $\rho(\lambda) \sim C_d \lambda^{d/2-1}$, leading to $\Gamma\left(\frac{d}{2}, f\right)$, so the exponent $3/2$ is the special case $d = 3$.

References

[1] Yehuda Pinchover and Jacob Rubinstein. *An Introduction to Partial Differential Equations*. Cambridge University Press, 2005.

[2] Matthias Brack and Rajat K. Bhaduri. *Semiclassical Physics*. Addison-Wesley, 1997.

[3] Yu. Safarov and D. Vassiliev. *The Asymptotic Distribution of Eigenvalues of Partial Differential Operators*. American Mathematical Society., 1997.

[4] V. Ya. Ivrii. Second term of the spectral asymptotic expansion of the laplace - beltrami operator on manifolds with boundary. *Functional Analysis and Its Applications*, 14(2):98–106, 1980.

[5] Michael Levitin, Dan Mangoubi, and Iosif Polterovich. *Topics in Spectral Geometry*. American Mathematical Society, 2023.

[6] Timothy Gowers, June Barrow-Green, and Imre Leader, editors. *The Princeton Companion to Mathematics*. Princeton University Press, Princeton and Oxford, 2008.

[7] H. P. W. Gottlieb. Eigenvalues of the laplacian for rectilinear regions. *The ANZIAM Journal*, 29(3):270–281, 1988.

[8] Jr. H. P. McKean and I. M. Singer. Curvature and the eigenvalues of the laplacian. *Journal of Differential Geometry*, 1(1-2):43–69, 1967.

[9] Radmila Bulajich Manfrino, José Antonio Gómez Ortega, and Rogelio Valdez Delgado. *Topics in Algebra and Analysis: Preparing for the Mathematical Olympiad*. Birkhäuser, 2015.

[10] Eldar Sultanow. 3d rendering of the rectangular box geometry. *renderings/box_a1.0_b1.5_c2.3.blend*, 2026. Blender rendering file, cone-operator-lab repository.

[11] Eldar Sultanow. Numerical generation of dirichlet laplacian eigenvalues on a rectangular box. *mathematica/Hearing_Box_GenerateEigenvalues.nb*, 2026. Mathematica notebook, cone-operator-lab repository.

[12] Eldar Sultanow. Stability landscape analysis and volcano surface visualization (3d). *mathematica/Hearing_Box_AnalyzeStabilitätsminimum.nb*, 2026. Mathematica notebook, cone-operator-lab repository.

[13] Carl M. Bender and Steven A. Orszag. *Advanced Mathematical Methods for Scientists and Engineers I: Asymptotic Methods and Perturbation Theory*. Springer, 1999.

[14] Eldar Sultanow. Stability plateau extraction and egg-contour fitting (2d). *python/notebooks/-Hearing_Box_ReconstructWeylCoeffs_HeatEquation_CalcStabilitaetsminimumA2-2D.ipynb*, 2026. Jupyter notebook, cone-operator-lab repository.

[15] Walter A. Strauss. *Partial Differential Equations: An Introduction*. John Wiley & Sons, 2 edition, 2008.

[16] Peter V. O'Neil. *Beginning Partial Differential Equations*. John Wiley & Sons, 2 edition, 2008.

[17] Les Piegl and Wayne Tiller. *The NURBS Book*. Springer, 2 edition, 1997.

[18] Georg Glaeser, Hellmuth Stachel, and Boris Odehnal. *The Universe of Conics*. Springer, 2 edition, 2024.

[19] Igor R. Shafarevich. *Basic Algebraic Geometry 1: Varieties in Projective Space*. Springer, 3 edition, 2013.

[20] Ulrich Görtz and Torsten Wedhorn. *Algebraic Geometry II: Cohomology of Schemes*. Springer, 2023.

[21] A. R. Forsyth. *Theory of functions of a complex variable*, volume 2. Dover, 3 edition, 1965.

[22] Robert J. Walker. *Algebraic Curves*. Springer, 1978.

[23] Maria Alberich-Carramiñana. *Geometry of the Plane Cremona Maps*. Springer, 2002.

Eldar Sultanow, Capgemini Deutschland GmbH, Nuremberg, Germany
Email address: eldar.sultanow@capgemini.com

Andreas Hatziliou, University of British Columbia, Department of Mathematics, 1984 Mathematics Rd, Vancouver BC, Canada
Email address: ahatzi@math.ubc.ca

Cornelius May, Capgemini Deutschland GmbH, Nuremberg, Germany
Email address: cornelius.may@capgemini.com